ISSN 1674-1056
http://cpb.iphy.ac.cn
http://iopscience.iop.org/cpb
中国物理 B
Chinese Physics
中国物理
Chinese Physics B

Solitary wave for a nonintegrable discrete nonlinear Schrödinger equation in nonlinear optical waveguide arrays

Li-Yuan Ma(马立媛), Jia-Liang Ji(季佳梁), Zong-Wei Xu(徐宗玮), Zuo-Nong Zhu(朱佐农)
Citation: Chin. Phys. B . 2018, 27(3): 030201. **doi:** 10.1088/1674-1056/27/3/030201

Journal homepage: http://cpb.iphy.ac.cn; http://iopscience.iop.org/cpb

What follows is a list of articles you may be interested in

Simulations of solitary waves of RLW equation by exponential B-spline Galerkin method

Melis Zorsahin Gorgulu, Idris Dag, Dursun Irk
Chin. Phys. B . 2017, 26(8): 080202. **doi:** 10.1088/1674-1056/26/8/080202

(2+1)-dimensional dissipation nonlinear Schrödinger equation for envelope Rossby solitary waves and chirp effect

Jin-Yuan Li(李近元), Nian-Qiao Fang(方念乔), Ji Zhang(张吉), Yu-Long Xue(薛玉龙), Xue-Mu Wang(王雪木), Xiao-Bo Yuan(袁晓博)
Chin. Phys. B . 2016, 25(4): 040202. **doi:** 10.1088/1674-1056/25/4/040202

A new model for algebraic Rossby solitary waves in rotation fluid and its solution

Chen Yao-Deng, Yang Hong-Wei, Gao Yu-Fang, Yin Bao-Shu, Feng Xing-Ru
Chin. Phys. B . 2015, 24(9): 090205. **doi:** 10.1088/1674-1056/24/9/090205

Exponential B-spline collocation method for numerical solution of the generalized regularized long wave equation

Reza Mohammadi
Chin. Phys. B . 2015, 24(5): 050206. **doi:** 10.1088/1674-1056/24/5/050206

Complex dynamical behaviors of compact solitary waves in the perturbed mKdV equation

Yin Jiu-Li, Xing Qian-Qian, Tian Li-Xin
Chin. Phys. B . 2014, 23(8): 080201. **doi:** 10.1088/1674-1056/23/8/080201

Solitary wave for a nonintegrable discrete nonlinear Schrödinger equation in nonlinear optical waveguide arrays*

Li-Yuan Ma(马立媛)[1], Jia-Liang Ji(季佳梁)[2], Zong-Wei Xu(徐宗玮)[3], and Zuo-Nong Zhu(朱佐农)[3,†]

[1] Department of Applied Mathematics, Zhejiang University of Technology, Hangzhou 310023, China
[2] School of Mathematics, Physics and Statistics, Shanghai University of Engineering Science, Shanghai 201620, China
[3] School of Mathematical Sciences, Shanghai Jiao Tong University, Shanghai 200240, China

(Received 24 August 2017; revised manuscript received 25 December 2017; published online 13 February 2018)

We study a nonintegrable discrete nonlinear Schrödinger (dNLS) equation with the term of nonlinear nearest-neighbor interaction occurred in nonlinear optical waveguide arrays. By using discrete Fourier transformation, we obtain numerical approximations of stationary and travelling solitary wave solutions of the nonintegrable dNLS equation. The analysis of stability of stationary solitary waves is performed. It is shown that the nonlinear nearest-neighbor interaction term has great influence on the form of solitary wave. The shape of solitary wave is important in the electric field propagating. If we neglect the nonlinear nearest-neighbor interaction term, much important information in the electric field propagating may be missed. Our numerical simulation also demonstrates the difference of chaos phenomenon between the nonintegrable dNLS equation with nonlinear nearest-neighbor interaction and another nonintegrable dNLS equation without the term.

Keywords: nonintegrable dNLS equation, solitary waves, chaos, nonlinear nearest-neighbor interaction

PACS: 02.30.Ik, 05.45.Yv **DOI:** 10.1088/1674-1056/27/3/030201

1. Introduction

As is well known, discrete soliton appears in a wide variety of physical areas, e.g., atomic chain[1,2] with on-site cubic nonlinearities, electrical lattices,[3] biophysics,[4,5] and in arrays of coupled nonlinear optical wave guides.[6,7] It has been demonstrated that a discrete nonlinear Schrödinger (dNLS) equation, integrable or nonintegrable, can be used as the models describing the discrete phenomena in the real physics. The dNLS describing the electric field propagating in nonlinear optical waveguide arrays was first introduced by Christodoulides and Joseph.[8] By using the formalism of coupled-mode theory and considering only nearest-neighbor interaction, they showed that the electric field propagating in the nonlinear optical waveguide obeys

$$\begin{aligned} &\mathrm{i}\frac{\partial E_n}{\partial z}+\beta E_n+c(E_{n+1}+E_{n-1})\\ &+\mu E_n(|E_{n+1}|^2+|E_{n-1}|^2)+\lambda E_n|E_n|^2=0, \end{aligned} \tag{1}$$

where the nonlinear term $\lambda|E_n|^2E_n$ describes the self-phase modulation that takes place in the nth waveguide, and the term $\mu E_n(|E_{n+1}|^2+|E_{n-1}|^2)$ arises from the nonlinear overlap of the adjacent modes. It is difficult to study the discrete model (1). However, in many cases, the self-phase-modulation term $\lambda|E_n|^2E_n$ dominates the nonlinear process. Hence, they set $\mu=0$, and discussed the nonintergable discrete NLS

$$\mathrm{i}\frac{\partial E_n}{\partial z}+c(E_{n+1}+E_{n-1}-2E_n)+\lambda|E_n|^2E_n=0. \tag{2}$$

The nonintergable dNLS also has applications in biophysics for explaining some of the fundamental questions, such as transfer, storage, and movement of vibrational energy in polypeptides.[4] The dNLS equation (2) has been investigated in terms of many aspects, including Hamiltonian analysis,[5] dynamics behaviors,[9–13] and discrete perturbation.[14] By using discrete Fourier transformation, Ablowitz and Musslimani constructed stationary and travelling soliton waves of dNLS equation (Eq. (2)).[14] However, as is well known, if we neglect the nonlinear nearest-neighbor interaction term, much important information, e.g., the shape of the wave, for the electric field propagating in nonlinear optical waveguide arrays, might be missed.

In this paper, we study the discrete model (1) which can be rewritten as

$$\begin{aligned} &\mathrm{i}\frac{\partial \phi_n}{\partial z}+\frac{\phi_{n+1}-2\phi_n+\phi_{n-1}}{h^2}\\ &+\alpha\phi_n(|\phi_{n+1}|^2+|\phi_{n-1}|^2)+\beta|\phi_n|^2\phi_n=0. \end{aligned} \tag{3}$$

We emphasize here that the nonintegrable dNLS equation (3) cannot be obtained by the reduction of Eq. (4) in Ref. [15]. The modulation stability of nonlinear plane-wave solutions of Eq. (3) is discussed.[16] By using discrete Fourier transformation, we will give numerical solitary waves for the two cases of stationary and traveling types, respectively. The stability analysis of stationary solitary waves will be discussed. It is shown that the nonlinear hopping term has great influence on the form of solitary wave. The shape of solitary wave is the

*Project supported by the National Natural Science Foundation of China (Grant Nos. 11671255 and 11701510), the Ministry of Economy and Competitiveness of Spain (Grant No. MTM2016-80276-P (AEI/FEDER, EU)), and the China Postdoctoral Science Foundation (Grant No. 2017M621964).

†Corresponding author. E-mail: znzhu@sjtu.edu.cn

© 2018 Chinese Physical Society and IOP Publishing Ltd

important information in the electric field propagating. We will demonstrate that the solitary wave possesses new behaviors, e.g., in the defocusing case, i.e., $2\alpha+\beta<0$, and there exists the discrete bright soliton. This quite contradicts the discrete integrable case, or the ones of continuous integrable systems. Furthermore, we also test the effectiveness of the nonintegrable NLS equation (3) as a discrete model for the NLS equation. Numerical simulation shows that the discrete model (3) is better than the model (2).

2. Stationary and traveling solitary waves from discrete Fourier transformation

In this section, by using the discrete Fourier transformation approach,[14] we will obtain numerical approximations of discrete localized stationary and traveling solitary waves for nonintegrable dNLS equation (3). The key point of the method is to transform a differential advance-delay equation into a nonlinear integral equation which can be solved numerically. The stability of stationary solitary waves will be conducted. We should remark here that though there is a standard method based on the solution of the nonlinear eigenvalue problem to find localized solutions of discrete systems (see e.g., Ref. [17]), in order to compare with the corresponding results of nonintegrable discrete NLS equation (2), we employ the discrete Fourier transformation approach to deal with Eq. (3).

2.1. Transform a differential advance-delay equation into a nonlinear integral equation

Setting ϕ_n in the form

$$\phi_n(z)=u(\xi)\,\mathrm{e}^{-\mathrm{i}\psi_n}, \tag{4}$$

where $\xi=nh-Vz$, $\psi_n=\eta nh-\omega z$, and $u(\xi)=F(\xi)+\mathrm{i}G(\xi)$, with V and ω being the soliton velocity and wave-number shift, respectively, equation (3) is reduced to the following differential advance-delay equation:

$$\begin{aligned}
&VG^{'}+\mathcal{D}_1F+\mathcal{D}_2G+\alpha F(E_++E_-)(F^2+G^2)\\
&+\beta(F^2+G^2)F=\omega F,\\
&-VF^{'}+\mathcal{D}_1G-\mathcal{D}_2F+\alpha G(E_++E_-)(F^2+G^2)\\
&+\beta(F^2+G^2)G=\omega G,
\end{aligned} \tag{5}$$

where prime denotes the derivative with respect to ξ and

$$\begin{aligned}
\mathcal{D}_1\mathcal{F}&=\frac{1}{h^2}[\cos(\eta h)(E_++E_-)\mathcal{F}-2\mathcal{F}],\\
\mathcal{D}_2\mathcal{G}&=\frac{\sin(\eta h)}{h^2}(E_+-E_-)\mathcal{G},
\end{aligned} \tag{6}$$

with $E_\pm X(\xi)=X(\xi\pm h)$. It is very difficult to find a solution to the system (5). To solve Eq. (5), we employ the discrete Fourier transformation. Introducing the discrete Fourier transform,

$$\begin{aligned}
\hat{F}(q)&=\sum_{m=-\infty}^{+\infty}F(mh)\,\mathrm{e}^{-\mathrm{i}qmh},\\
F(nh)&=\frac{h}{2\pi}\int_{-\pi/h}^{\pi/h}\hat{F}(q)\,\mathrm{e}^{\mathrm{i}qnh}\,\mathrm{d}q,
\end{aligned} \tag{7}$$

then the system (5) can be transformed into the nonlinear integral equations as follows:

$$\begin{aligned}
\hat{F}(q)&=\frac{\Omega_1(q)Q_1[\hat{F},\tilde{G}](q)+\Omega_2(q)Q_2[\hat{F},\tilde{G}](q)}{\Omega_1^2(q)-\Omega_2^2(q)},\\
\tilde{G}(q)&=\frac{\Omega_1(q)Q_2[\hat{F},\tilde{G}](q)+\Omega_2(q)Q_1[\hat{F},\tilde{G}](q)}{\Omega_1^2(q)-\Omega_2^2(q)},
\end{aligned} \tag{8}$$

where $\tilde{G}(q)\equiv\mathrm{i}\hat{G}(q)$ and,

$$\begin{aligned}
\Omega_1(q)&=\omega+\frac{2}{h^2}[1-\cos(hq)\cos(\eta h)],\\
\Omega_2(q)&=qV+\frac{2}{h^2}\sin(hq)\sin(\eta h),\\
Q_1[\hat{F},\tilde{G}](q)&=\frac{\beta h^2}{4\pi^2}[\hat{F}\times(\hat{F}\times\hat{F}-\tilde{G}\times\tilde{G})](q)\\
&\quad+\frac{\alpha h^2}{2\pi^2}(\hat{F}\times Q_0[\hat{F},\tilde{G}])(q),\\
Q_2[\hat{F},\tilde{G}](q)&=\frac{\beta h^2}{4\pi^2}[\tilde{G}\times(\hat{F}\times\hat{F}-\tilde{G}\times\tilde{G})](q)\\
&\quad+\frac{\alpha h^2}{2\pi^2}(\tilde{G}\times Q_0[\hat{F},\tilde{G}])(q),\\
Q_0[\hat{F},\tilde{G}](q)&=(\hat{F}_\mathrm{A}\times\hat{F}_\mathrm{A}-\hat{F}_\mathrm{B}\times\hat{F}_\mathrm{B}\\
&\quad-\tilde{G}_\mathrm{A}\times\tilde{G}_\mathrm{A}+\tilde{G}_\mathrm{B}\times\tilde{G}_\mathrm{B})(q),
\end{aligned} \tag{9}$$

with

$$\begin{aligned}
&(\hat{L}\times\hat{M}\times\hat{N})(q)=\iint\mathrm{d}q_1\,\mathrm{d}q_2\hat{L}(q_1)\hat{M}(q_2)\hat{N}(q-q_1-q_2),\\
&\hat{F}_\mathrm{A}(q)=\hat{F}(q)\cos(qh),\quad \hat{F}_\mathrm{B}(q)=\hat{F}(q)\sin(qh),\\
&\tilde{G}_\mathrm{A}(q)=\tilde{G}(q)\cos(qh),\quad \tilde{G}_\mathrm{B}(q)=\tilde{G}(q)\sin(qh).
\end{aligned}$$

It should be remarked that when we derive Eq. (8), we have used the following discrete Fourier transformation for $F(\xi)$, $\xi=nh-Vz$, and its property

$$\begin{aligned}
\hat{F}(q)&=\sum_{m=-\infty}^{+\infty}F(mh-Vz)\,\mathrm{e}^{-\mathrm{i}q(mh-Vz)},\\
F(\xi)&=\frac{h}{2\pi}\int_{-\pi/h}^{\pi/h}\hat{F}(q)\,\mathrm{e}^{\mathrm{i}q(nh-Vz)}\,\mathrm{d}q,\\
\hat{F}(f'(\xi))&=\mathrm{i}q\hat{F}(f(\xi)).
\end{aligned} \tag{10}$$

Furthermore, in order to obtain a solution for the integral equation (8), we will employ the Petviashvili method, or modified Neumann iteration scheme.[17–20]

2.2. Stationary solitary wave

To obtain discrete localized stationary solitary wave, we set $V=0$, $\eta=0$, $\omega=\omega_s$, and $G=0$. Then system (8) is reduced to the following nonlinear integral equation:

$$\begin{aligned}\hat{F}(q) &= \frac{h^2}{4\pi^2\Omega(q)}\big[\beta(\hat{F}\times\hat{F}\times\hat{F})\\ &\quad +2\alpha(\hat{F}\times\hat{F}_{\rm A}\times\hat{F}_{\rm A}-\hat{F}\times\hat{F}_{\rm B}\times\hat{F}_{\rm B})\big](q)\\ &\triangleq \mathcal{K}_{\omega_s}[\hat{F}(q)],\end{aligned}\tag{11}$$

where $\Omega(q)=\omega_s+2[1-\cos(hq)]/h^2$ is the frequency of the linear excitations. We construct function sequences $\{\hat{F}_n(q)\}$ defined by

$$\begin{aligned}&\hat{F}_{n+1}(q)=\left|\frac{\theta(\hat{F}_n)}{\delta(\hat{F}_n)}\right|^{3/2}\mathcal{K}_{\omega_s}[\hat{F}_n(q)],\quad n\geqslant 0,\\ &\theta=\int\hat{F}_n^2(q)\,{\rm d}q,\quad \delta=\int\hat{F}_n(q)\mathcal{K}_{\omega_s}[\hat{F}_n(q)]\,{\rm d}q.\end{aligned}\tag{12}$$

Numerical simulation shows that by choosing the proper values for the parameters, then as $n\to\infty$

$$\left|\frac{\theta(\hat{F}_n(q))}{\delta(\hat{F}_n(q))}\right|\to 1,$$

and the function sequence $\hat{F}_n(q)$ is convergent. We set $\hat{F}_n(q)\to\hat{F}_s(q)$ as $n\to\infty$. Then $\hat{F}_s(q)$ is a fixed point of nonlinear integrable equation (11), and its inverse Fourier transformation $F(nh)$ is an approximate solution of nonintegrable dNLS equation (3).

Let us give a numerical example with the parameters and initial value being: $\alpha=2$, $\beta=1$, $\omega_s=1$, $h=0.25$, $\hat{F}_0(q)=1$. The result of the numerical simulation is given in Table 1.

Table 1. Result of the numerical simulation, where we take $\hat{F}_s(q)=\hat{F}_{18}(q)$, and the term $|\theta_n/\delta_n|$ and the error $\||\hat{F}_n|-|\hat{F}_s|\|_{L^2}$ are described.

n	$\lvert\theta_n/\delta_n\rvert$	$\||\hat{F}_n\|-\lvert\hat{F}_s\|\|_{L^2}$
10	1.000292257	3.487392294×10^{-3}
11	1.000142013	1.689079794×10^{-3}
12	1.000069007	8.151729560×10^{-4}
13	1.000033529	3.905044349×10^{-4}
14	1.000016295	1.841653477×10^{-4}
15	1.000007918	8.389725678×10^{-5}
16	1.000003848	3.517549057×10^{-5}
17	1.000001869	1.149495739×10^{-5}
18	1.000000909	/

In the following numerical examples, we take the values of the parameters which include three cases of $\alpha+\beta>0$, $\alpha+\beta<0$, and $\alpha+\beta=0$. They correspond respectively to focusing NLS, defocusing NLS, and LS equations.

Figure 1 gives the shapes of the stationary solitary wave with the different nonlinear nearest-neighbor interaction term parameter α in Fourier domain and physical space, where the nonintegrable term β, wave-number shift ω_s, and the lattice spacing h are fixed. We find that the nonlinear nearest-neighbor interaction term parameter α has influence on the soliton's amplitude. When the nonlinear term parameter $\alpha=-0.5$, the amplitude of the soliton attains the maximum. When α increases from -0.5 and α decreases from -0.5, the amplitude decreases monotonically in both two cases.

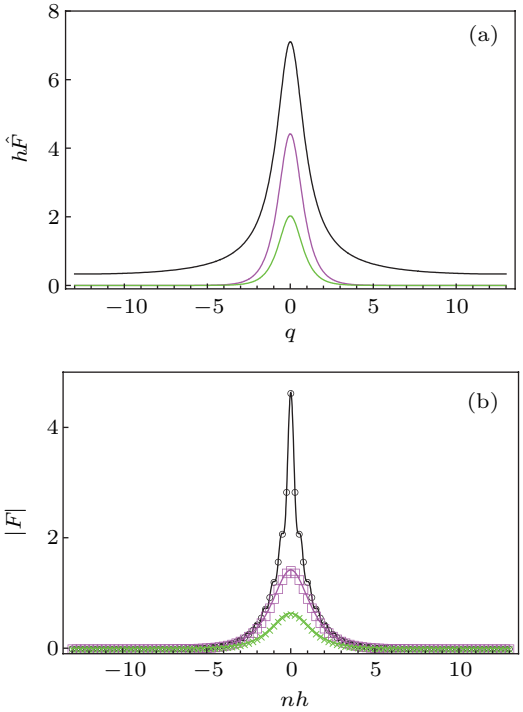


Fig. 1. (color online) Stationary solitons when $\omega_s=1$, $\beta=1$, $h=0.25$. (a) Fourier space. (b) Physical space. Black: $\alpha=-0.5$; magenta: $\alpha=0$; green: $\alpha=2$. Every circle, box and fork marked on the respective line represents the values of $|F(nh)|$.

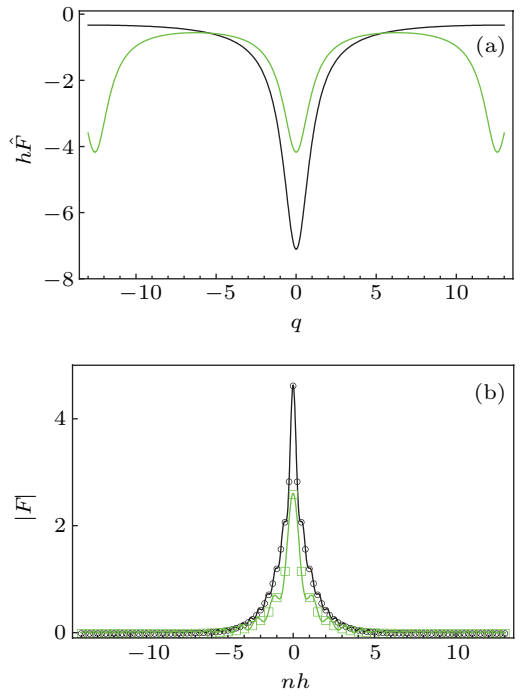


Fig. 2. (color online) Stationary solitons with $\omega_s=1$, $\beta=-1$, and $\alpha=0.5$. Black: $h=0.25$; green: $h=0.5$. (a) Fourier space. (b) Physical space. Note that the background in panel (a) is nonzero. The property of nonlinear hopping α is displayed in panel (b), and the value of $F(nh)$ tends to be zero as $|n|\to\infty$ in physical space. The values of $|F(nh)|$ in each line are marked by signs of circles and boxes, respectively.

This type of solution is called discrete breathers.[21,22]

Figure 2 describes an oscillate solitary wave, where $\omega_s = 1$, $\beta = -1$, $\alpha = 0.5$ $(2\alpha+\beta = 0)$, with two different values of lattice spacing, $h = 0.25$, and $h = 0.5$.

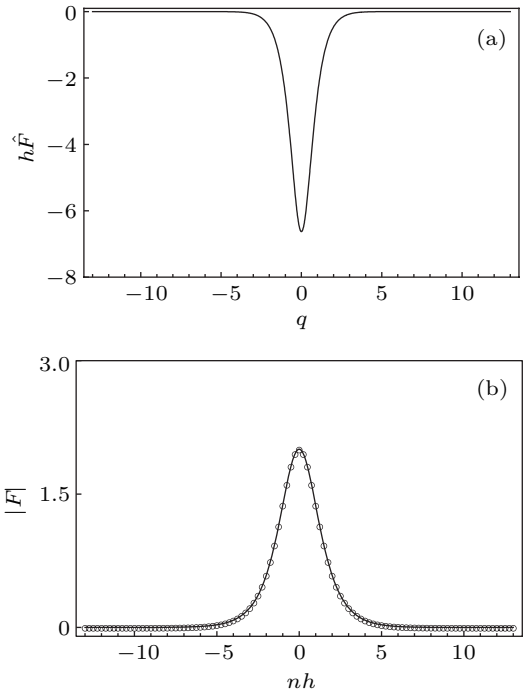


Fig. 3. Stationary bright soliton with $\omega_s = 1$ and $h = 0.25$, $\alpha = 0.5$, $\beta = -0.5$. (a) Fourier space. (b) Physical space. Every circle signed on the line stands for the values of $|F(nh)|$.

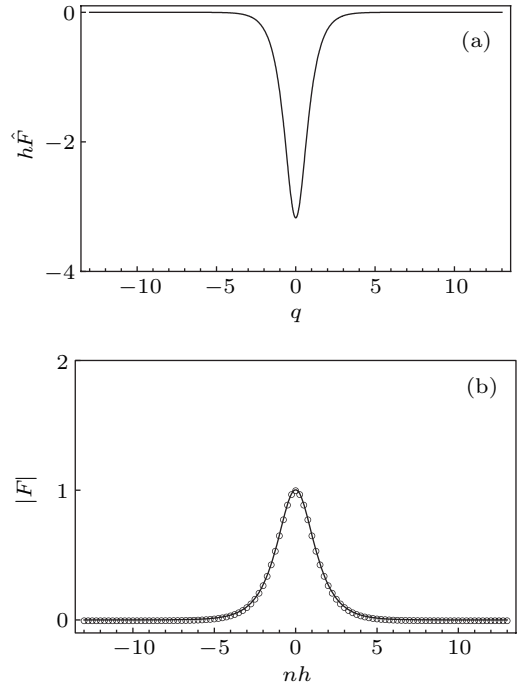


Fig. 4. Stationary bright soliton with $\omega_s = 1$, $\beta = -1$, and $h = 0.25$, $\alpha = -0.5$. (a) Fourier space. (b) Physical space. Every circle marked on the line represents the values of $|F(nh)|$.

Figure 3 gives a discrete bright soliton, where we choose parameters $\omega_s = 1$ and $h = 0.25$, $\alpha = 0.5$, $\beta = -0.5$ $(2\alpha+\beta > 0)$. However, under the situation $\alpha < 0$ and $\beta < 0$, we can also obtain the bright soliton, which is shown in Fig. 4, where the parameters $\omega_s = 1$, $\beta = -1$, and $h = 0.25$, $\alpha = -0.5$ $(2\alpha+\beta < 0)$. This result contradicts with the ones in the discrete integrable cases or the ones of continuous integrable systems.

Figure 5 shows an oscillate solitary wave in the case of $2\alpha+\beta > 0$. We can see that the structures of solitary waves for nonintegrable discrete NLS equation (3) with the nonlinear nearest-neighbor interaction are much more richer than those of solitary waves for nonintegrable discrete NLS equation (2) without the term. As is well known, the shape of solitary wave is the important information in the study of the electric field propagating. When we use the nonintegrable discrete NLS equation (3) with the nonlinear nearest-neighbor interaction as the model of electric field propagating, we can modulate the shape of the wave by choosing the self-phase modulation and the term of the nonlinear overlap of the adjacent modes.

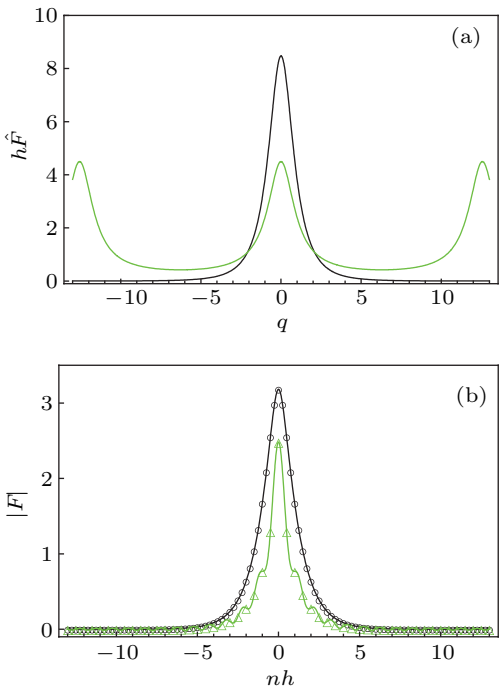


Fig. 5. (color online) Stationary solitons with $\omega_s = 1$, $\beta = 1$, $\alpha = -0.4$. (a) Fourier space. (b) Physical space. The property of nonlinear hopping α is displayed in panel (b). The value of $|F(nh)|$ tends to be zero as $|n| \to \infty$ in physical space. Black: $h = 0.25$; green: $h = 0.5$.

2.3. Analysis of linear stability for stationary solitary wave

In this subsection, following the idea in Ref. [23], we examine the linear stability of stationary solutions of the nonintegrable discrete NLS equation (3). For convenience, we set $\varepsilon = 1/h^2$. We have known that the nonintegrable discrete NLS equation (3) admits the following localized stationary solution:

$$\phi_n(z) = u_n \mathrm{e}^{\mathrm{i}\omega z}, \tag{13}$$

where u_n is a localized real function (i.e., $u_n \to 0$ as $|n| \to \infty$) and satisfies the difference equation

$$\varepsilon(u_{n+1} - 2u_n + u_{n-1}) - \omega u_n$$

$$+\alpha u_n(u_{n+1}^2+u_{n-1}^2)+\beta u_n^3=0. \tag{14}$$

To study the linear stability of solution (13), we consider the behavior of the stationary solution under small perturbations. Inserting the perturbed solution

$$\phi_n(z)=(u_n+\tilde{\phi}_n(z))\,\mathrm{e}^{\mathrm{i}\omega z},\quad \tilde{\phi}_n(z)\ll 1, \tag{15}$$

into Eq. (3) and dropping the terms of quadratic and higher order in $\tilde{\phi}_n(z)$, we derive a linear equation with respect to $\tilde{\phi}_n(z)$,

$$\begin{aligned}&\mathrm{i}\frac{\partial\tilde{\phi}_n(z)}{\partial z}+\varepsilon\left(\tilde{\phi}_{n+1}(z)-2\tilde{\phi}_n(z)+\tilde{\phi}_{n-1}(z)\right)\\&-\omega\tilde{\phi}_n(z)+\beta u_n^2(2\tilde{\phi}_n(z)+\tilde{\phi}_n^*(z))\\&+\alpha\big(u_nu_{n+1}(\tilde{\phi}_{n+1}(z)+\tilde{\phi}_{n+1}^*(z))\\&+u_nu_{n-1}(\tilde{\phi}_{n-1}(z)+\tilde{\phi}_{n-1}^*(z))\\&+(u_{n+1}^2+u_{n-1}^2)\tilde{\phi}_n(z)\big)=0.\end{aligned} \tag{16}$$

By substituting the solution in the form of normal modes with the eigenvalue λ

$$\tilde{\phi}_n(z)=f_n\,\mathrm{e}^{\lambda z}+g_n^*\,\mathrm{e}^{\lambda^* z} \tag{17}$$

into Eq. (16), and introducing the variable transformation

$$f_n=v_n+w_n,\quad g_n=v_n-w_n, \tag{18}$$

we obtain the discrete linear eigenvalue problem

$$\boldsymbol{L}_n\boldsymbol{Y}_n=-\mathrm{i}\lambda\boldsymbol{Y}_n, \tag{19}$$

where

$$\boldsymbol{L}_n=\begin{pmatrix}0 & L_{0,n}\\ L_{1,n} & 0\end{pmatrix},\quad \boldsymbol{Y}_n=\begin{pmatrix}v_n\\ w_n\end{pmatrix}, \tag{20}$$

and

$$\begin{aligned}L_{0,n}&=\varepsilon(E-2+E^{-1})\\&\quad-\omega+\alpha(u_{n+1}^2+u_{n-1}^2)+\beta u_n^2,\end{aligned} \tag{21}$$

$$\begin{aligned}L_{1,n}&=\varepsilon(E-2+E^{-1})\\&\quad-\omega+\alpha(2u_n(u_{n+1}E+u_{n-1}E^{-1})\\&\quad+u_{n+1}^2+u_{n-1}^2)+3\beta u_n^2.\end{aligned} \tag{22}$$

There exists a continuous spectrum as $|n|\to\infty$ with the eigenfunction $\boldsymbol{Y}_n$ given by $\boldsymbol{Y}_n=(c_1,c_2)^{\mathrm{T}}\mathrm{e}^{\mathrm{i}kn}$, where k is a real wavenumber, (c_1,c_2) are constants. Solving Eq. (19) gives the continuous eigenvalues $\lambda=\pm\mathrm{i}(\omega+2\varepsilon(1-\cos k))$. Thus the continuous spectrum of Eq. (19) extends over the intervals $[\omega,\omega+4\varepsilon]$ and $[-(\omega+4\varepsilon),-\omega]$ on the imaginary axis.

Note that $\lambda=0$ is a discrete eigenvalue which has a discrete eigenfunction $\boldsymbol{Y}_{n,1}$ and a generalized discrete eigenfunction $\boldsymbol{Y}_{n,2}$,

$$\boldsymbol{Y}_{n,1}=\begin{pmatrix}0\\ u_n\end{pmatrix},\quad \boldsymbol{Y}_{n,2}=\begin{pmatrix}\dfrac{\mathrm{d}u_n}{\mathrm{d}\omega}\\ 0\end{pmatrix}. \tag{23}$$

We remark here that the so-called generalized discrete eigenfunction refers to the relation: $\boldsymbol{L}_n\boldsymbol{Y}_{n,2}=\boldsymbol{Y}_{n,1}$.

To look for the nonzero discrete eigenvalue of Eq. (19) through the numerical method, we truncate the lattice n to $-N\le n\le N$, then the infinite-dimensional discrete eigenvalue problem (19) reduces to the case of the finite-dimensional one

$$\begin{aligned}&\mathrm{i}\begin{pmatrix}\boldsymbol{O} & \boldsymbol{A}_{(2N+1)\times(2N+1)}\\ \boldsymbol{B}_{(2N+1)\times(2N+1)} & \boldsymbol{O}\end{pmatrix}\\&\times\begin{pmatrix}(\boldsymbol{V}_n)_{(2N+1)\times1}\\ (\boldsymbol{W}_n)_{(2N+1)\times1}\end{pmatrix}=\lambda\begin{pmatrix}(\boldsymbol{V}_n)_{(2N+1)\times1}\\ (\boldsymbol{W}_n)_{(2N+1)\times1}\end{pmatrix},\end{aligned} \tag{24}$$

where $\boldsymbol{V}_n$, $\boldsymbol{W}_n$, $\boldsymbol{A}$, and $\boldsymbol{B}$ are, respectively

$$\boldsymbol{V}_n=(v_{-N},v_{-N+1},\ldots,v_N)^{\mathrm{T}},\quad \boldsymbol{W}_n=(w_{-N},w_{-N+1},\ldots,w_N)^{\mathrm{T}},$$

$$\boldsymbol{A}=\begin{pmatrix}\Delta_{-N} & \varepsilon & & & & & & \\ \varepsilon & \Delta_{-N+1} & \varepsilon & & & & & \\ & \varepsilon & \Delta_{-N+2} & \varepsilon & & & & \\ & & \ddots & \ddots & \ddots & & & \\ & & & \ddots & \ddots & \varepsilon & & \\ & & & & \varepsilon & \Delta_{N-1} & \varepsilon & \\ & & & & & \varepsilon & \Delta_N & \end{pmatrix}$$

with $\Delta_j=\alpha(u_{j+1}^2+u_{j-1}^2)+\beta u_j^2-\omega-2\varepsilon$ $(j=-N,\ldots,N)$.

$$\boldsymbol{B}=\begin{pmatrix}\Omega_{-N} & \Theta_{-N} & & & & & & \\ \Theta_{-N} & \Omega_{-N+1} & \Theta_{-N+1} & & & & & \\ & \Theta_{-N+1} & \Delta_{-N+2} & \Theta_{-N+2} & & & & \\ & & \ddots & \ddots & \ddots & & & \\ & & & \ddots & \ddots & \Theta_{N-2} & & \\ & & & & \Theta_{N-2} & \Omega_{N-1} & \Theta_{N-1} & \\ & & & & & \Theta_{N-1} & \Omega_N & \end{pmatrix},$$

with $\Omega_j = \alpha(u_{j+1}^2 + u_{j-1}^2) + 3\beta u_j^2 - \omega - 2\varepsilon$, $\Theta_j = \varepsilon + 2\alpha u_j u_{j+1}$ $(j = -N, \ldots, N)$.

Let us give out the discrete spectrum of the different stationary solitary waves corresponding to the cases of Figs. 1–5. As described in Ref. [23], a necessary condition for the stability of stationary solitary waves is that $\mathrm{Re}\lambda \leq 0$ for all eigenvalues. A sufficient condition for the instability is that at least a discrete eigenvalue λ, s.t., $\mathrm{Re}\lambda > 0$. Considering the accuracy of numerical simulation, we set $h = 0.25$. Then taking $\omega = 1$ yields the intervals $i[1, 65]$ and $i[-65, -1]$ for the continuous spectrum which is described by the green line in the figures. We choose $N = 52$ in Figs. 6–11.

For the stationary solitary wave in Fig. 6(a) with $2\alpha+\beta = 0$, $\alpha < 0$, the discrete spectrum of the linearization operator L_n contains two pairs of real eigenvalues in Figs. 6(b) and 6(c). The real eigenvalues are

$$\lambda_1 = -12.1295, \quad \lambda_2 = 12.1295,$$
$$\lambda_3 = -0.0097, \quad \lambda_4 = 0.0097.$$

Since there exist two positive real eigenvalues, the corresponding perturbed solution will exponentially grow with z, i.e., the stationary solitary wave in Fig. 6(a) is linearly unstable.

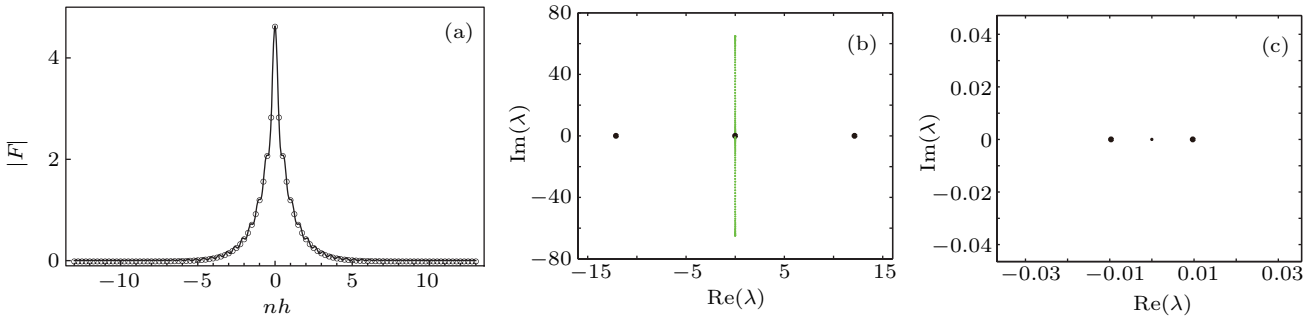


Fig. 6. (color online) (a) Stationary solitary wave in physical space with parameters $\omega_s = 1$, $\alpha = -0.5$, $\beta = 1$, $h = 0.25$. (b) Spectrum of linearization operator L_n for the stationary solitary wave (a) contains two pairs of real eigenvalues. Green continuous spectrum, black discrete spectrum. (c) A pair of nonzero real discrete eigenvalues near the zero: $\lambda_3 = -0.0097$ and $\lambda_4 = 0.0097$.

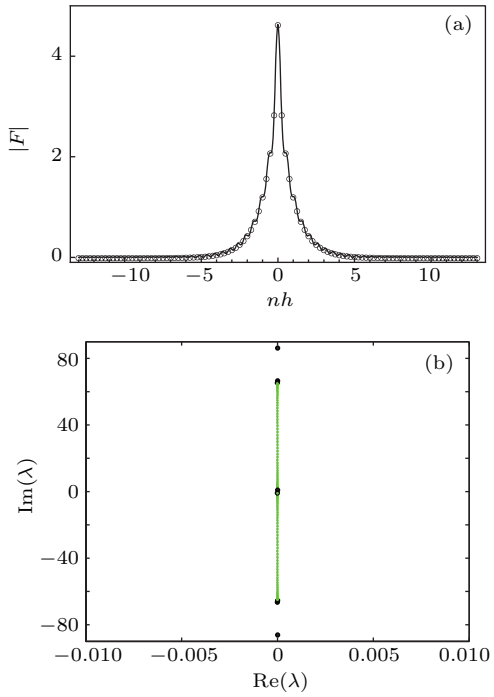


Fig. 7. (color online) (a) Stationary solitary wave in physical space with parameters $\omega_s = 1$, $\alpha = 0.5$, $\beta = -1$, $h = 0.25$. (b) Spectrum of the linearization operator L_n for the stationary solitary wave (a) contains four pairs of internal modes.

For the stationary solitary wave in Fig. 7(a) $2\alpha + \beta = 0$, $\beta < 0$, four pairs of discrete eigenvalues are located at the imaginary axis, which are called internal modes. They are

$$\lambda_2 = -\lambda_1 = 86.1750\mathrm{i}, \quad \lambda_4 = -\lambda_3 = 66.5296\mathrm{i},$$
$$\lambda_6 = -\lambda_5 = 65.4042\mathrm{i}, \quad \lambda_8 = -\lambda_7 = 0.9217\mathrm{i}.$$

In this case, the perturbed term $\tilde{\phi}_n(z)$ will oscillate with z.

A pair of real eigenvalues and three pairs of internal modes for the stationary solitary wave in Fig. 8(a) with $2\alpha + \beta > 0$, $\beta < 0$ are given in Fig. 8(b). The real eigenvalues are $\lambda_1 = -0.0208$ and $\lambda_2 = 0.0208$. Three pairs of internal modes are

$$\lambda_4 = -\lambda_3 = 0.0222\mathrm{i}, \quad \lambda_6 = -\lambda_5 = 65.2992\mathrm{i},$$
$$\lambda_8 = -\lambda_7 = 67.3812\mathrm{i}.$$

The positive real eigenvalue leads to the linear instability of the solitary wave in Fig. 8(a).

A pair of internal modes $\lambda_1 = -66.0164\mathrm{i}$ and $\lambda_2 = 66.0164\mathrm{i}$ appear in Fig. 9(b) as the parameters are $\omega_s = 1$, $\alpha = -0.5$, $\beta = -1$, $h = 0.25$. Like the case in Fig. 7(b), this indicates that the perturbed term $\tilde{\phi}_n(z)$ will also oscillate with z.

For the stationary solitary wave in Fig. 10(a) with parameters $\omega_s = 1$, $\alpha = -0.4$, $\beta = 1$, $h = 0.25$ $(2\alpha + \beta > 0, \alpha < 0)$, a pair of real eigenvalues $\lambda_1 = -0.0373$, $\lambda_2 = 0.0373$, and two pairs of internal modes

$$\lambda_3 = -0.0830\mathrm{i}, \quad \lambda_4 = 0.0830\mathrm{i},$$
$$\lambda_5 = -0.9099\mathrm{i}, \quad \lambda_6 = 0.9099\mathrm{i}$$

are obtained, see Figs. 10(b) and 10(c). Due to the occurrence of the positive real eigenvalue λ_2, this stationary solution is linearly unstable.

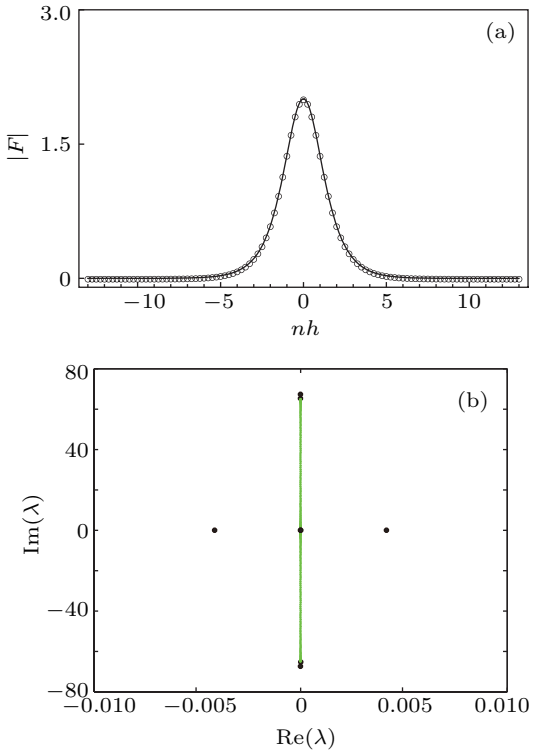


Fig. 8. (color online) (a) Stationary solitary wave in physical space with parameters $\omega_s = 1$, $\alpha = 0.5$, $\beta = -0.5, h = 0.25$. (b) Spectrum of the linearization operator L_n for the stationary solitary wave (a) contains a pair of real eigenvalues and three pairs of internal modes.

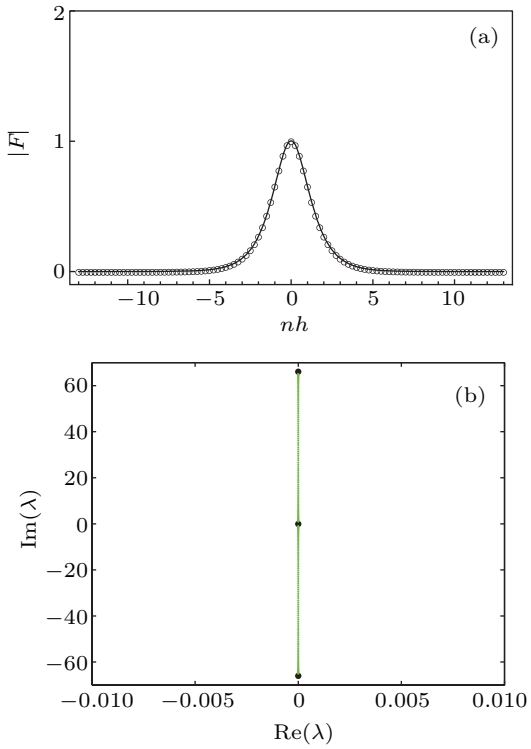


Fig. 9. (color online) (a) Stationary solitary wave in physical space with parameters $\omega_s = 1$, $\alpha = -0.5$, $\beta = -1$, $h = 0.25$. (b) Spectrum of the linearization operator L_n for the solution in panel (a) contains a pair of internal modes.

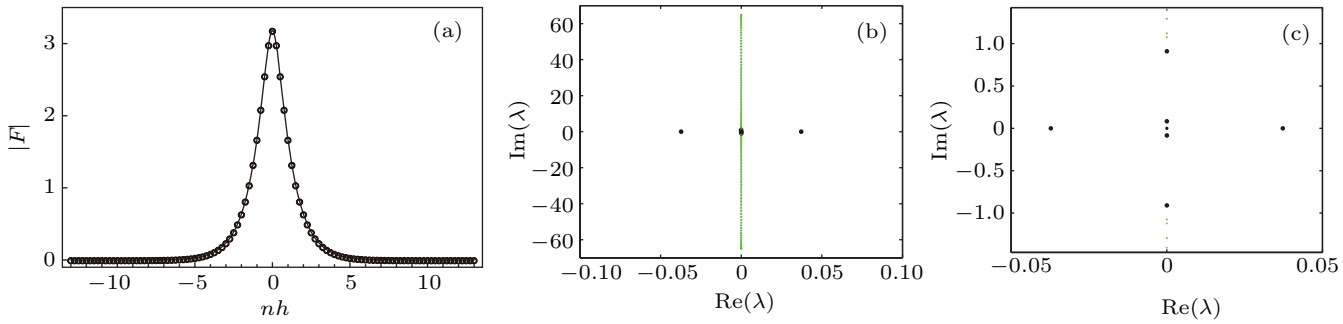


Fig. 10. (color online) (a) Stationary solitary wave in physical space with parameters $\omega_s = 1$, $\alpha = -0.4$, $\beta = 1$, $h = 0.25$. (b), (c) Discrete spectrum contains a pair of real eigenvalues and two pairs of internal modes.

To compare with the linear stability of stationary solution (13) for nonintegrable discrete NLS equation (3) and an integrable discrete NLS equation

$$\mathrm{i}\frac{\partial \phi_n}{\partial z} + \frac{\phi_{n+1} - 2\phi_n + \phi_{n-1}}{h^2} + |\phi_n|^2(\phi_{n+1} + \phi_{n-1}) = 0, \tag{25}$$

we investigate the linear stability of the stationary solution of Eq. (25). The localized real function u_n in stationary solution (13) satisfies the following difference equation:

$$\varepsilon(u_{n+1} - 2u_n + u_{n-1}) - \omega u_n + u_n^2(u_{n+1} + u_{n-1}) = 0. \tag{26}$$

Under the action of the perturbed solution (15), the corresponding operators for discrete linear eigenvalue problem (19) is

$$L_{0,n} = \varepsilon(E - 2 + E^{-1}) - \omega + u_n^2(E + E^{-1}), \tag{27}$$

$$L_{1,n} = \varepsilon(E - 2 + E^{-1}) - \omega + u_n^2(E + E^{-1}) + 2u_n(u_{n+1} + u_{n-1}). \tag{28}$$

Thus, the reduced finite-dimensional discrete eigenvalue problem (24) becomes

$$\mathrm{i}\begin{pmatrix} \boldsymbol{O} & \boldsymbol{A}_{(2N+1)\times(2N+1)} \\ \boldsymbol{A}_{(2N+1)\times(2N+1)} & \boldsymbol{O} \end{pmatrix} \times \begin{pmatrix} (\boldsymbol{V}_n)_{(2N+1)\times 1} \\ (\boldsymbol{W}_n)_{(2N+1)\times 1} \end{pmatrix} = \lambda \begin{pmatrix} (\boldsymbol{V}_n)_{(2N+1)\times 1} \\ (\boldsymbol{W}_n)_{(2N+1)\times 1} \end{pmatrix}, \tag{29}$$

where the matrix $\boldsymbol{A}$ is

$$\boldsymbol{A}=\begin{pmatrix} -2\varepsilon-\omega & \varepsilon+u_{-N}^2 & & & & & \\ \varepsilon+u_{-N+1}^2 & -2\varepsilon-\omega & \varepsilon+u_{-N+1}^2 & & & & \\ & \varepsilon+u_{-N+2}^2 & -2\varepsilon-\omega & \varepsilon+u_{-N+2}^2 & & & \\ & & \ddots & \ddots & \ddots & & \\ & & & \ddots & \ddots & \varepsilon+u_{N-2}^2 & \\ & & & & \varepsilon+u_{N-1}^2 & -2\varepsilon-\omega & \varepsilon+u_{N-1}^2 \\ & & & & & \varepsilon+u_{N}^2 & -2\varepsilon-\omega \end{pmatrix}.$$

The linearization operator L_n of the stationary solitary wave has only zero discrete eigenvalue except the continuous spectrum (see Fig. 11(b)). It should be remarked that as mentioned in Ref. [17], the appearance of nonzero discrete eigenvalues in the linearization spectrum of solitary waves is an important phenomenon of nonintegrable equations.

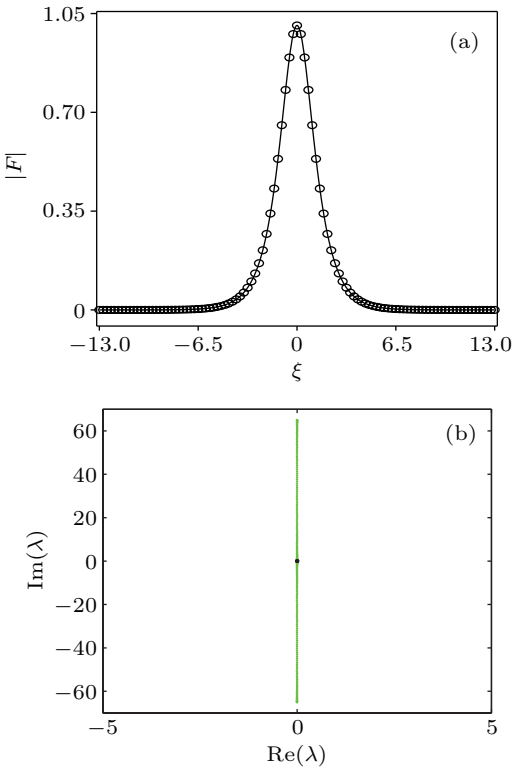


Fig. 11. (color online) (a) Stationary solitary wave of integrable discrete NLS equation (25) with parameters $\omega_s=1$ and $h=0.25$. (b) Continuous spectrum and zero eigenvalue.

2.4. Traveling solitary waves

To find the traveling solitary wave of the dNLS equation (3), we take the following iteration scheme:

$$\begin{aligned}\hat{F}_{n+1}(q) &= \left|\frac{\theta_1(\hat{F}_n,\tilde{G}_n)}{\delta_1(\hat{F}_n,\tilde{G}_n)}\right|^{3/2} \times\frac{\Omega_1(q)Q_1[\hat{F}_n,\tilde{G}_n](q)+\Omega_2(q)Q_2[\hat{F}_n,\tilde{G}_n](q)}{\Omega_1^2(q)-\Omega_2^2(q)},\\ \tilde{G}_{n+1}(q) &= \left|\frac{\theta_1(\hat{F}_n,\tilde{G}_n)}{\delta_1(\hat{F}_n,\tilde{G}_n)}\right|^{3/2} \times\frac{\Omega_1(q)Q_2[\hat{F}_n,\tilde{G}_n](q)+\Omega_1(q)Q_2[\hat{F}_n,\tilde{G}_n](q)}{\Omega_1^2(q)-\Omega_2^2(q)},\end{aligned} \tag{30}$$

where

$$\begin{aligned}\theta_1 &= \int\left(\hat{F}_n^2(q)+\tilde{G}_n^2(q)\right)\mathrm{d}q,\\ \delta_1 &= \int\frac{1}{\Omega_1^2(q)-\Omega_2^2(q)}\big\{\hat{F}_n(q)(\Omega_1(q)Q_1[\hat{F}_n,\tilde{G}_n](q)\\ &\quad+\Omega_2(q)Q_2[\hat{F}_n,\tilde{G}_n](q))\\ &\quad+\tilde{G}_n(q)(\Omega_1(q)Q_2[\hat{F}_n,\tilde{G}_n](q)\\ &\quad+\Omega_2(q)Q_1[\hat{F}_n,\tilde{G}_n](q))\big\}\mathrm{d}q.\end{aligned} \tag{31}$$

Similarly, by numerical simulation, as $n\to\infty$, we have

$$\left|\frac{\theta_1(\hat{F}_n,\tilde{G}_n)}{\delta_1(\hat{F}_n,\tilde{G}_n)}\right|\to 1,$$

and function sequences $\{\hat{F}_n(q)\}$ and $\{\tilde{G}_n(q)\}$ are convergent. We set $\hat{F}_n(q)\to\hat{F}_s(q)$ and $\tilde{G}_n(q)\to\tilde{G}_s(q)$ as $n\to\infty$. Then $\hat{F}_s(q),\tilde{G}_s(q)$ is a fixed point of nonlinear integrable equation (8), and their inverse Fourier transformation $F(\xi),G(\xi)$ is an approximate solution of Eq. (5).

Let us give two examples of numerical simulations for nonlinear integral equation (30).

Example 1 We consider the following parameters and initial functions:

$$\alpha=-3,\quad \beta=1,\quad \omega=1,\quad h=0.5,\quad V=-0.25,\quad \eta=0.5,$$
$$\hat{F}_0(q)=\mathrm{sech}(q),\quad \hat{G}_0(q)=\mathrm{sech}(q)\tanh(q).$$

The result of the numerical simulation is given in Table 2.

In this case, a typical traveling soliton solution to Eq. (3) is presented in Fig. 12. In Figs. 12(a) and 12(b), we can observe that the change of the parameter α has an influence on

Table 2. Result of the numerical simulation, where we take $\hat{F}_s(q)=\hat{F}_9(q)$, $\hat{G}_s(q)=\hat{G}_9(q)$, and the term $|\theta_n/\delta_n|$ and the error $\||\hat{F}_n|-|\hat{F}_s|\|_{L^2}$, $\||\hat{G}_n|-|\hat{G}_s|\|_{L^2}$ are described.

n	$\lvert\theta_n/\delta_n\rvert$	$\||\hat{F}_n\|-\|\hat{F}_s\|\|_{L^2}$	$\||\hat{G}_n\|-\|\hat{G}_s\|\|_{L^2}$
0	8.877893522	3.352658448	0.9175705942
1	0.9817287753	0.4555124406	0.4894667216
2	1.009863536	0.2126252935	0.1980691767
3	1.006922399	0.09453384938	0.08453467201
4	1.003372246	0.04079576537	0.03641463045
5	1.001488911	0.01719842545	0.01557783237
6	1.000632970	0.007014725747	0.006484957196
7	1.000264618	0.002653843929	0.002506429867
8	1.000109738	0.0007929615513	0.0007636846252
9	1.000045315	/	/

the amplitude of the soliton mode. Figure 12(c) describes a wave, which travels to the left. The hopping term has much more influence on the traveling solitons when $|2\alpha+\beta|$ approaches zero. Figure 13 displays the hopping property in the traveling soliton mode. From Fig. 13(d), we see that the amplitude of the soliton has some slight oscillations at the two sides of the wave. Similar results with stationary cases are obtained when $|2\alpha+\beta|$ is near zero. The modes of the traveling solitons have oscillations when $|2\alpha+\beta|$ is in a small neighborhood of zero.

Example 2 We take $\omega=1$, $\alpha=-0.5$, $\beta=1$, $\eta=0.5$, $V=-0.25$, $h=0.5$, $\hat{F}_0(q)=\cos(q)\,\mathrm{sech}(q)$, $\hat{G}_0(q)=\mathrm{sech}(q)\tanh(q)$. The result of the numerical simulation is given by Table 3.

Table 3. Result of the numerical simulation, where we take $\hat{F}_s(q)=\hat{F}_{32}(q)$, $\hat{G}_s(q)=\hat{G}_{32}(q)$, and the term $|\theta_n/\delta_n|$ and the error $\||\hat{F}_n|-|\hat{F}_s|\|_{L^2}$, $\||\hat{G}_n|-|\hat{G}_s|\|_{L^2}$ are described.

n	$\lvert\theta_n/\delta_n\rvert$	$\||\hat{F}_n\rvert-\lvert\hat{F}_s\|\|_{L^2}$	$\||\hat{G}_n\rvert-\lvert\hat{G}_s\|\|_{L^2}$
20	1.000134342	0.1273209351	0.2424569932
21	1.000111199	0.1078827133	0.2062115148
22	1.000107203	0.09085135334	0.1740868791
23	1.000095399	0.07581796199	0.1456743590
24	1.000089525	0.06259654921	0.1205206177
25	1.000082143	0.05093576049	0.09826955517
26	1.000076907	0.04066248241	0.07858087147
27	1.000071721	0.03160105568	0.06116518909
28	1.000067527	0.02361028880	0.04575937073
29	1.000063686	0.01655973903	0.03213361113
30	1.000060417	0.01033852186	0.02008244443
31	1.000057506	0.004847348592	0.009424846514
32	1.000054972	/	/

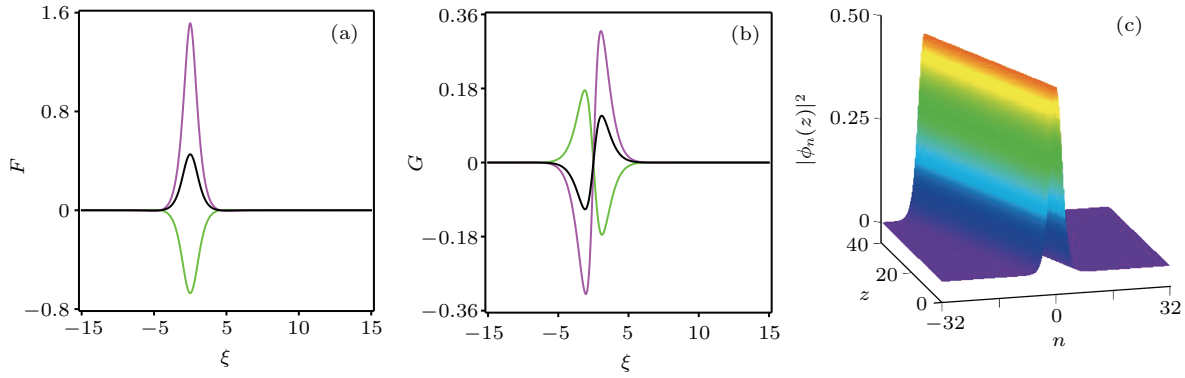


Fig. 12. (color online) Traveling soliton. (a), (b) Parameters are chosen to be $\omega=1$, $\beta=1$, $h=0.5$, $\eta=0.5$, $V=-0.25$. $\alpha=-3$ (green); $\alpha=0$ (pink); $\alpha=5$ (black). (c) Evolution of a traveling soliton with parameters being $\omega=1$, $\beta=1$, $h=0.5$, $\eta=0.5$, $V=-0.25$, and $\alpha=-3$.

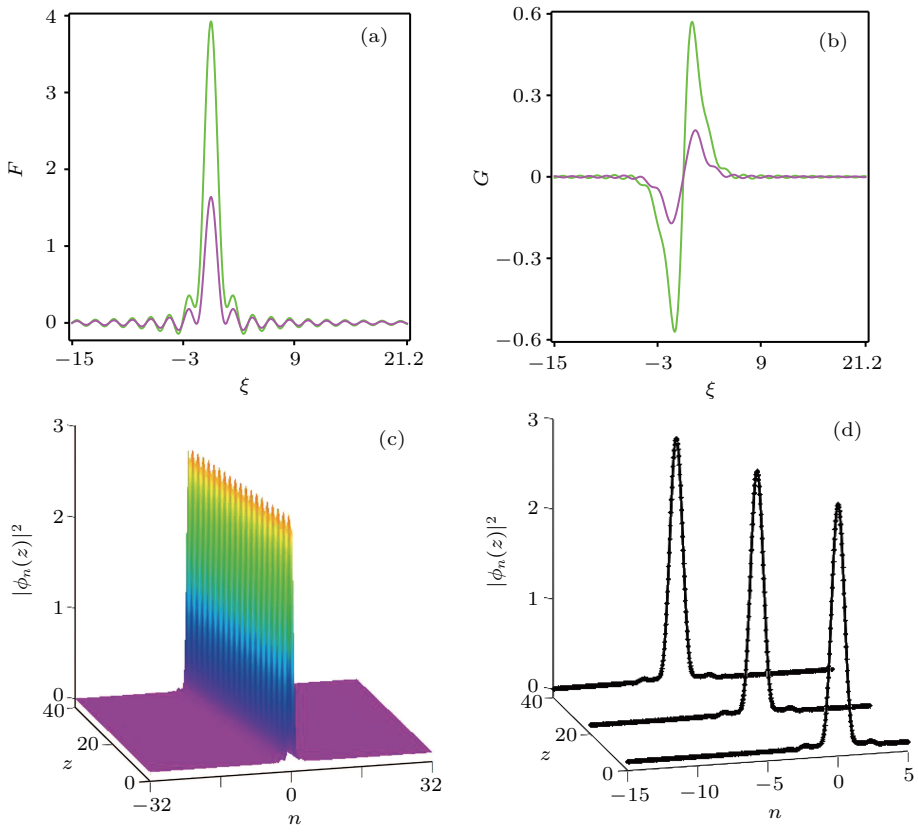


Fig. 13. (color online) Traveling solitons when $\omega=1$, $\beta=1$, $\eta=0.5$, $V=-0.155$, $\alpha=-0.5$. $h=0.5$ (green); $h=1$ (pink). Evolution of the traveling soliton is given in 3-dimensional figure (c) under the situation of $\omega=1$, $\beta=1$, $\eta=0.5$, $V=-0.155$, $\alpha=-0.5$, and $h=1$. (d) Several soliton modes at different values of z.

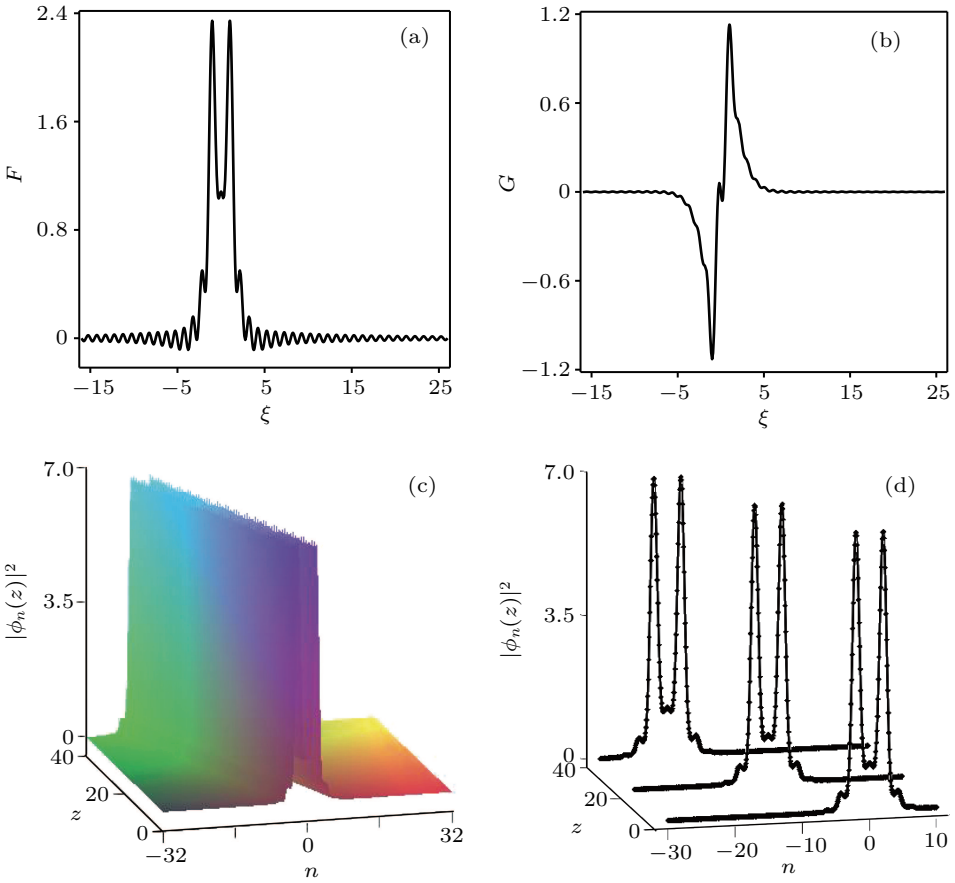


Fig. 14. (color online) Traveling soliton with parameters being $\omega = 1$, $\beta = 1$, $\eta = 0.5$, $V = -0.25$, $\alpha = -0.5$, and $h = 0.5$, and initial data being $\hat{F}_0(q) = \cos(q)\,\mathrm{sech}(q)$, $\tilde{G}_0(q) = \mathrm{sech}(q)\tanh(q)$. Panels (a) and (b) show the shape of $F(\xi)$ and $G(\xi)$ in physical space, respectively. Panel (c) displays the evolution of the traveling soliton. Panel (d) gives several soliton modes at different values of z.

Figures 14(a) and 14(b) give the shapes of $F(\xi)$ and $G(\xi)$. Figures 14(c) and 14(d) describe the evolution of the traveling soliton. The traveling soliton possesses new behaviors, e.g., it has two peaks in the shape, and the oscillations occur not only at the edges of the wave, but also in the middle of the wave.

3. Chaos phenomenon between the nonintegrable dNLS equation with the term of nonlinear nearest-neighbor interaction and another nonintegrable dNLS equation without the term

In this section, we will show a difference of chaos phenomenon between the nonintegrable dNLS equation with the term of nonlinear nearest-neighbor interaction and another nonintegrable dNLS equation without the term. Herbst and Ablowitz[24] considered the Cauchy problem for NLS,

$$\mathrm{i}q_t + q_{xx} + \gamma|q|^2 q = 0, \tag{32}$$

with periodic boundary condition $q(x+L,t) = q(x,t)$, and the initial condition $q(x,0) = a[1+\varepsilon\cos(\mu_n x)]$ and $\mu_n = 2\pi n/L$. They gave a numerical computation for the Cauchy problem. They proposed integrable discrete scheme (25) of NLS and the following nonintegrable discrete scheme:

$$\mathrm{i}q_{n,t} + \frac{q_{n+1} + q_{n-1} - 2q_n}{h^2} + \gamma|q_n|^2 q_n = 0, \tag{33}$$

with the periodic boundary conditions $q_{n+N} = q_n$ and $h = L/N$. It has been demonstrated that the nonintegrable discrete scheme produces a chaotic solution for intermediate levels of mesh refinement, e.g., $N = 32$. However, chaos disappears when the discretization is fine enough, e.g., $N = 50$, and the convergence to a quasiperiodic solution is obtained. Numerical simulation has been performed by choosing $\gamma = 4$, $L = 2\sqrt{2}\pi$, $q(x,0) = 0.5[1 + 0.1\cos(2\pi x/L)]$ (see Ref. [24]). Here, we would like to test what happens if the discrete model is a nonintegrable discrete NLS equation (3). Let us change Eq. (3) into the following form:

$$\mathrm{i}\frac{\partial\phi_n}{\partial t} + \frac{\phi_{n+1} - 2\phi_n + \phi_{n-1}}{h^2} + \frac{\alpha\gamma}{2}\phi_n(|\phi_{n+1}|^2 + |\phi_{n-1}|^2) + \beta\gamma|\phi_n|^2\phi_n = 0, \tag{34}$$

where $\alpha + \beta = 1$. Our numerical simulation (time integration is performed by the Runge–Kutta–Merson method) shows that model (34) is better than the discrete model (33), i.e., model (2). In fact, by numerical simulation, we find that the nonintegrable discrete scheme (34) still produces a chaotic

solution for intermediate levels of mesh refinement. However, due to the integrable term $\frac{\alpha\gamma}{2}\phi_n(|\phi_{n+1}|^2+|\phi_{n-1}|^2)$, the chaotic solution evolves gradually to a quasiperiodic solution with the integrable term increasing. For example, when $N=8$, from Fig. 15, we can see that the chaotic solution occurs. However, chaotic impact decreases with the term $\frac{\alpha\gamma}{2}\phi_n(|\phi_{n+1}|^2+|\phi_{n-1}|^2)$ gradually increasing. Furthermore, when mesh is refined to be $N=32$, if we choose $\alpha=0$, or $\alpha=1/5$, $\beta=4/5$, chaotic solutions still exist. However, if we choose $\alpha=1/3$ and $\beta=2/3$, the chaos disappears and the solution evolves in a quasiperiodic way (see Fig. 16). This implies that the existence of chaos relates closely to the level of mesh refinement and the discrete model. The term of nonlinear nearest-neighbor interaction has significant influence on the disappearance of the chaos. We thus think that the discrete NLS model (34) is better than the discrete NLS model (33) in the sense that the convergence to a quasiperiodic solution for the Cauchy problem of NLS needs less number of grid points N. We should emphasize again that nonintegrable discrete model (34) has a solitary wave solution, and yields a chaos phenomenon for the Cauchy problem of the NLS equation. The chaotic solution evolves gradually to the quasiperiodic solution with integrable term increasing. If $\beta=0$, the model (34) is integrable. Using the integrable scheme, a chaos phenomenon for the Cauchy problem of the NLS equation does not occur.

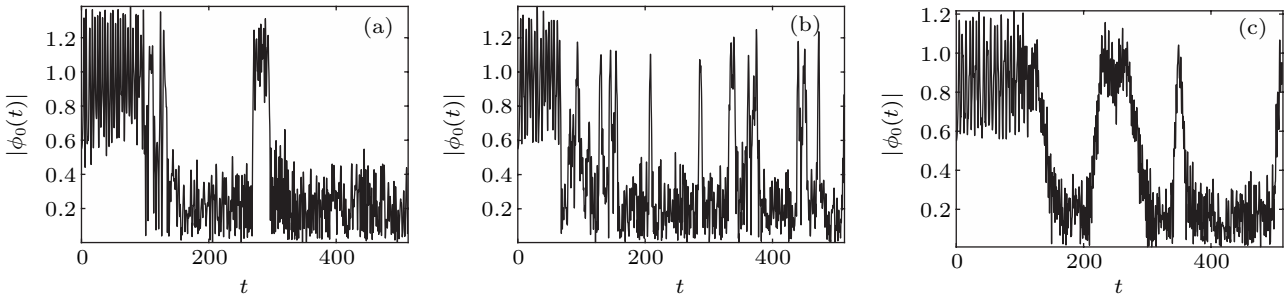


Fig. 15. Time evolution of the modulus of the solution for nonintegrable discrete NLS scheme (34). $N=8$. (a) $\alpha=1/3$, $\beta=2/3$; (b) $\alpha=1/2$, $\beta=1/2$; (c) $\alpha=2/3$, $\beta=1/3$.

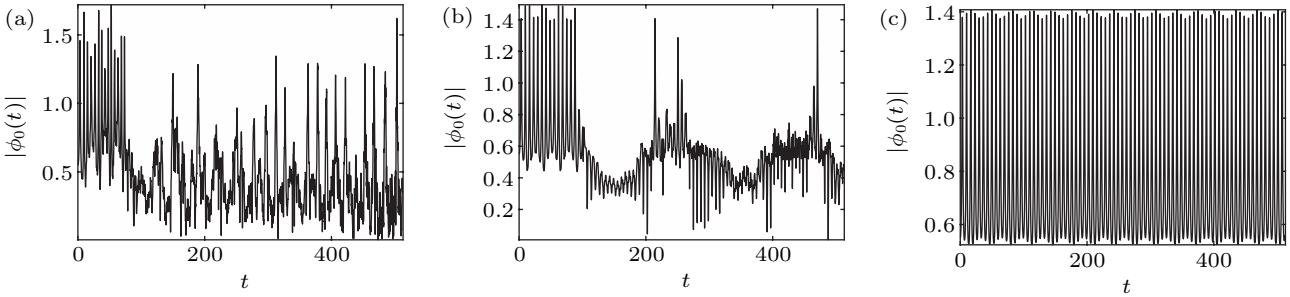


Fig. 16. Time evolution of the modulus of the solution for nonintegrable discrete NLS scheme (34). $N=32$. (a) $\alpha=0$, $\beta=1$; (b) $\alpha=1/5$, $\beta=4/5$; (c) $\alpha=1/3$, $\beta=2/3$.

4. Conclusions

In this paper, we have investigated a nonintegrable discrete nonlinear Schrödinger equation with the term of nonlinear nearest-neighbor interaction, which occurred in coupled waveguide arrays. By using discrete Fourier transformation and numerical simulation, we have obtained its localized stationary and traveling soliton solutions. The stability of stationary solitary wave has been analyzed. We have shown that the nonlinear nearest-neighbor interaction term has much more influence on the soliton modes. It has been demonstrated that the nonintegrable discrete nonlinear Schrödinger equation possesses new behaviors, e.g., for defocusing case ($2\alpha+\beta<0$), there exists discrete bright soliton. This is an interesting result, since it contradicts with the discrete or continuous integrable cases. We have also shown that a difference of chaos phenomenon between the nonintegrable dNLS equation with nonlinear nearest-neighbor interaction term (3) and nonintegrable dNLS equation (2) without the term. It has been demonstrated by numerical simulation that discrete NLS scheme (3) is better than the discrete NLS model (2). The term of nonlinear nearest-neighbor interaction in the discrete NLS scheme (3) has a significant influence on the disappearance of the chaos for the Cauchy problem of NLS equation.

References

[1] Scott A C and Macneil L 1983 *Phys. Lett. A* **98** 87
[2] Sievers A J and Takeno S 1988 *Phys. Rev. Lett.* **61** 970
[3] Marquii P, Bilbault J M and Remoissenet M 1995 *Phys. Rev. E* **51** 6127
[4] Davydov A S 1973 *J. Theor. Biol.* **38** 559

[5] Cai D, Bishop A R and Gronbech-Jensen N 1994 *Phys. Rev. Lett.* **72** 591
[6] Eisenberg H, Silberberg Y, Morandotti R, Boyd A and Aitchison J 1998 *Phys. Rev. Lett.* **81** 3383
[7] Morandotti R, Peschel U, Aitchison J, Eisenberg H and Silberberg Y 1999 *Phys. Rev. Lett.* **83** 2726
[8] Christodoulides D N and Joseph R J 1988 *Opt. Lett.* **13** 794
[9] Gómez-Gardeñes J and Floría L M 2004 *Chaos* **14** 1130
[10] Pando L C L and Doedel E J 2004 *Phys. Rev. E* **69** 036603
[11] Pando L C L and Doedel E J 2005 *Phys. Rev. E* **71** 056201
[12] Pando L C L and Doedel E J 2007 *Phys. Rev. E* **75** 016213
[13] Pando L C L and Doedel E J 2009 *Physica D* **238** 687
[14] Ablowitz M J, Musslimani Z H and Biondini G 2002 *Phys. Rev. E* **65** 026602
[15] Öster M, Johansson M and Eriksson A 2003 *Phys. Rev. E* **67** 056606
[16] Rojas-Rojas S, Vicencio R A, Molina M I and Abdullaev F Kh 2011 *Phys. Rev. A* **84** 033621
[17] Yang J 2010 *Nonlinear Waves in Integrable and Nonintegrable Systems* (Society for Industrial and Applied Mathematics, Philadelphia) pp. 163–168, 359–366
[18] Petviashvili V I 1976 *Sov. J. Plasma Phys.* **2** 257
[19] Ablowitz M J and Biondini G 1998 *Opt. Lett.* **23** 1668
[20] Pelinovsky D E and Stepanyants Y A 2004 *SIAM J. Numer. Anal.* **42** 1110
[21] Flach S and Willis C R 1998 *Phys. Rep.* **295** 181
[22] Flach S and Gorbach A V 2008 *Phys. Rep.* **467** 1
[23] Eilbeck J C, Lomdahl P S and Scott A C 1985 *Physica D* **16** 318
[24] Herbst B M and Ablowitz M J 1989 *Phys. Rev. Lett.* **62** 2065